Matter and Radiation at Extremes | RESEARCH ARTICLE | pubs.aip.org/aip/mre

Generating a tunable narrow electron beam comb via laser-driven plasma grating

Cite as: Matter Radiat. Extremes 8, 064001 (2023); doi: 10.1063/5.0151883
Submitted: 25 March 2023 • Accepted: 1 August 2023 •
Published Online: 13 September 2023

Hetian Yang,[1,2] Jingwei Wang,[2] Shixia Luan,[2,a)] Ke Feng,[2] Wentao Wang,[2,a)] and Ruxin Li[2,3]

AFFILIATIONS

[1] College of Science, University of Shanghai for Science and Technology, Shanghai 200093, People's Republic of China
[2] State Key Laboratory of High Field Laser Physics and CAS Center for Excellence in Ultra-Intense Laser Science, Shanghai Institute of Optics and Fine Mechanics (SIOM), Chinese Academy of Sciences (CAS), Shanghai 201800, People's Republic of China
[3] School of Physical Science and Technology, ShanghaiTech University, Shanghai 200031, People's Republic of China

[a)] **Authors to whom correspondence should be addressed:** sxluan@siom.ac.cn and wwt1980@siom.ac.cn

ABSTRACT

We propose a novel approach for generating a high-density, spatially periodic narrow electron beam comb (EBC) from a plasma grating induced by the interference of two intense laser pulses in subcritical-density plasma. We employ particle-in-cell (PIC) simulations to investigate the effects of cross-propagating laser pulses with specific angles overlapping in a subcritical plasma. This overlap results in the formation of a transverse standing wave, leading to a spatially periodic high-density modulation known as a plasma grating. The electron density peak within the grating can reach several times the background plasma density. The charge imbalance between electrons and ions in the electron density peaks causes mutual repulsion among the electrons, resulting in Coulomb expansion and acceleration of the electrons. As a result, some electrons expand into vacuum, forming a periodic narrow EBC with an individual beam width in the nanoscale range. To further explore the formation of the nanoscale EBC, we conduct additional PIC simulations to study the dependence on various laser parameters. Overall, our proposed method offers a promising and controlled approach to generate tunable narrow EBCs with high density.

I. INTRODUCTION

The interaction of multiple laser beams with plasmas has revealed various nonlinear effects, exhibiting novel features and finding numerous applications in different interaction configurations. For instance, four-wave mixing can result in phase-conjugating reflection,[1] and the use of two laser pulses can accelerate energetic particles.[2–7] Attosecond x-ray pulses can also be generated,[8] and terahertz radiation can be produced using a two-color laser scheme.[9,10] These interactions can occur when the laser beams are either parallel or crossed at specific angles. Moreover, recent studies have demonstrated that the intersection of two nonrelativistic laser beams with a plasma can induce a stable grating-like electron density modulation called a plasma Bragg grating (PBG).[11–14] This grating has diverse applications, including the manipulation of ultrashort intense laser pulses,[15–17] generation of electron bunches,[18] production of high-density electrons,[19] and triggering of electron injection in the laser wakefield.[20] However, when the intensity of the pump lasers reaches relativistic levels, new nonlinear phenomena arise during the interaction process.

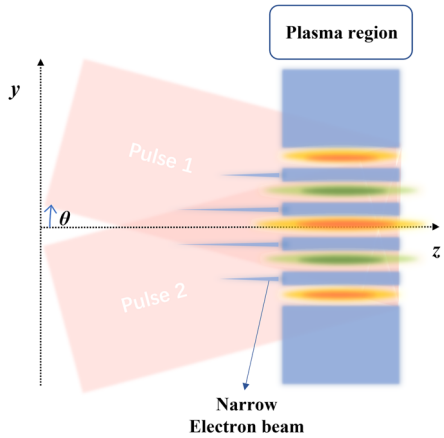

FIG. 1. Schematic of the proposed scheme. Two intense laser pulses interact on a subcritical density ($n_0 = 0.1n_c$) plasma layer at an angle $\theta = 10°$.

In this work, we propose a novel method for generating a high-density narrow electron beam comb (EBC) in the presence of a plasma grating. Our approach involves the interaction of two cross-propagating laser pulses at specific angles with critical-density plasmas. When these intense laser pulses intersect in the plasma, they create an interference field in the region of overlap, leading to the formation of an electron plasma grating. This grating introduces a charge imbalance between electrons and ions, resulting in strong mutual repulsion among the electrons. This repulsion causes Coulomb expansion of the electrons, with some of them expanding into the vacuum. Under the influence of the transverse standing wave field, a periodic accelerated EBC is generated. Our research demonstrates that the interference field can effectively guide and collimate these electron beams, allowing them to stably propagate for tens of femtoseconds. Furthermore, the width of the individual electron beams along the y direction can be reduced to the nanoscale range, with energy levels reaching several MeV and density levels reaching the critical density of the initial plasma. Additionally, the characteristics of the EBC can be tailored by adjusting the initial laser parameters.

II. EBC GENERATION

Figure 1 illustrates the proposed EBC scheme based on a plasma grating. The scheme is simulated using a 2D3V particle-in-cell (PIC) method with the LAPINE code.[21] The simulation involves two circularly polarized (CP) laser pulses, with the same strength parameter $a_L = 2$, wavelength $\lambda = 800$ nm, spot radius $b = 10\lambda_0$, and pulse duration $\tau = 30T_0$, where $\lambda_0 = 1$ μm is the unit of the simulation and T_0 is the laser period normalized with respect to λ_0. At $t = 0$, the two CP laser pulses intersect on the left side $(z = 0)$ of the plasma target at an angle $\theta = 10^\circ$. The peak intensity of the laser is 8.56×10^{18} W/cm^2. The plasma target consists of a uniform subcritical

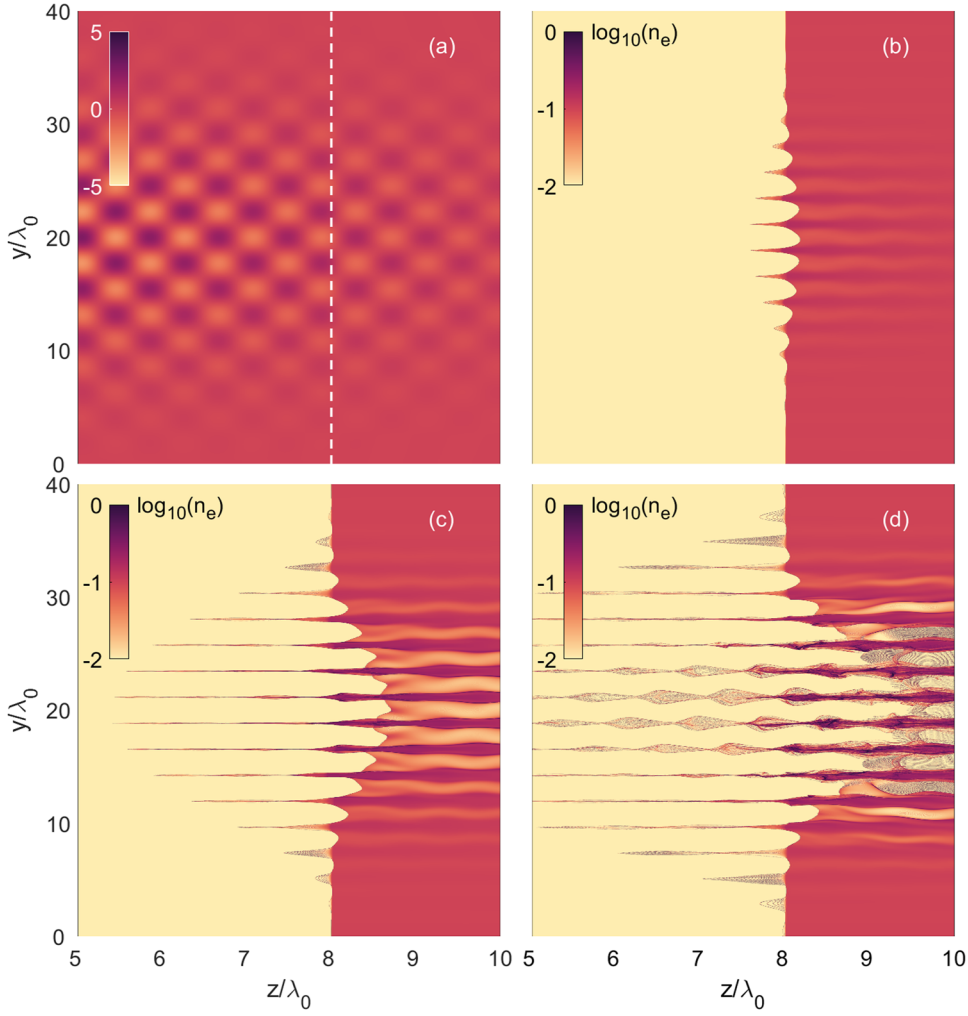

FIG. 2. (a) Snapshot of normalized laser light field $a_L(y, z, t)$ at time $t = 14T_0$. (b)–(d) Snapshots of electron density at times $t = 14T_0$, $18T_0$, and $22T_0$, respectively.

density plasma layer with density $n_0 = 0.1n_c$ and thickness $15\lambda_0$, where $n_c = 1.1 \times 10^{21}/\lambda_0^2$ cm^{-3} is the critical density. The plasma layer is located in $8 < z/\lambda_0 < 23$. The simulation box is $40\lambda_0 \times 25\lambda_0$, containing a 8000 × 5000 grid, with 16 ions and 16 electrons per cell. The ion–electron mass ratio is 1836.

To simulate the generation of the EBC, we first consider the propagation of laser pulses through a subcritical density plasma. Figure 2 illustrates the evolution of the EBC, showing snapshots of the normalized laser light field $a_L(y,z,t)$ at time $t = 14T_0$ [Fig. 2(a)] and the electron density at different times $t = 14T_0$, $18T_0$, and $22T_0$ [Fig. 2(b)–2(d)]. As the two laser pulses propagate forward and intersect on the plasma target at $z = 8\lambda_0$, their y components overlap and induce an interference field. We observe that the ponderomotive force of the interference field starts to expel electrons from the high-intensity regions, causing them to accumulate in the wave nodes and form a narrow density peak with a density several times higher than the background plasma. Subsequently, a spatially periodic modulation in electron density, known as an electron plasma grating,[11] is driven by the ponderomotive force, as depicted in Fig. 2(b). During this period, the massive ions remain stationary while the local non-neutrality of charge is established. The unneutralized electrons within the narrow high-density electron peak interact through mutual repulsion, triggering the Coulomb expansion process and inducing their acceleration. Some electrons move transversely and neutralize with the ions, while some move forward, sustaining the persistent Coulomb expansion. Additionally, a portion of backward-moving electrons overflows the target surface, forming an EBC.

At a later time $t = 18T_0$, under the continuous influence of the ponderomotive force of the interference field, most electrons between the peaks of the electron plasma grating are expelled from the high-intensity regions, resulting in the formation of several electron cavities, as observed in Fig. 2(c). Notably, the Coulomb expansion process of electrons persists from the density peak. We can observe the electron beams continuously emerging from the target surface with a speed of ~0.6c, while the electron density ripple structures induced by the transverse neutralization effect of electrons and ions begin to manifest in the plasma layer. The single electron beam of the EBC is compressed to an extremely narrow width in the nanoscale range under the guidance of the standing field in the y direction. The EBC can stably propagate longitudinally in vacuum for tens of femtoseconds. Eventually, the mutual repulsion among the electrons leads to dissipation of the electron bunches, as shown in Fig. 2(d).

We now further explore the detailed process of generation of the EBC. In Fig. 3, we observe the normalized laser light field $a_L(y,z,t)$ and electron density along the y direction at (a) $z = 9.5\lambda_0$ and (b) $z = 7.74\lambda_0$ at time $t = 18T_0$. Figure 3(a) illustrates the periodic standing field and the density distribution of the electron plasma grating. The ponderomotive force of the standing field expels the electrons located in the wave antinodes from the high-intensity regions. As a result, these electrons accumulate in the wave nodes, giving rise to the formation of a plasma grating. The period of this grating, as seen in Fig. 3(a), is ~2.3 μm, and the density of the electron peak is several times higher than the initial plasma density. Figure 3(b) shows the periodic standing field and density distribution of the EBC at $z = 7.74\lambda_0$ in vacuum. The period of the standing wave remains the same as in the plasma layer. Notably, the width of an individual electron beam in the y direction is compressed to about 52 nm (the electron beam width mentioned later refers to the y direction). The densities of these electron beams can approach the critical density.

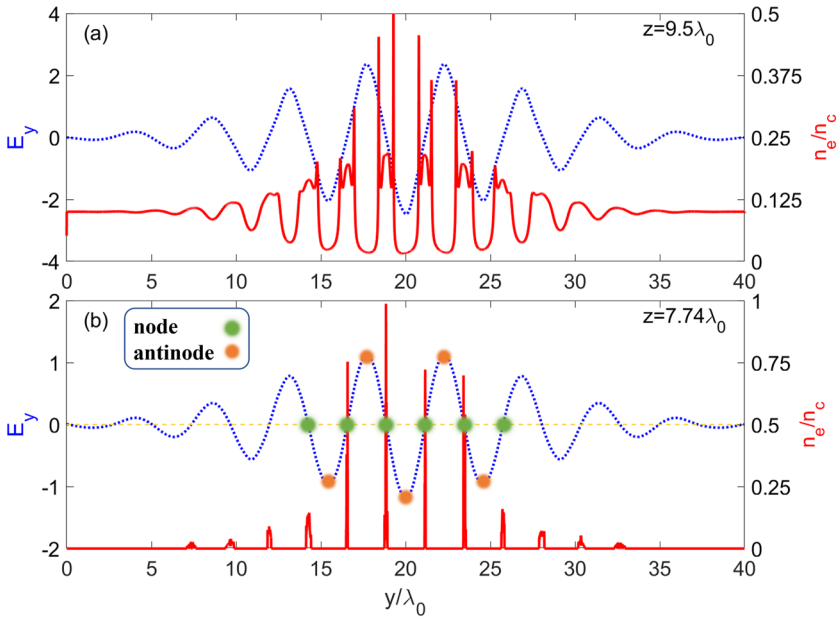

FIG. 3. Normalized laser light field $a_L(y,z,t)$ (blue dotted line) and electron density (red solid line) along the y direction at (a) $z = 9.5\lambda_0$ and (b) $z = 7.74\lambda_0$ at time $t = 18T_0$.

III. DEPENDENCE OF EBC ON LASER PARAMETERS

In the analysis of EBC generation, the spatial distribution of the EBC is intricately connected to the plasma grating, which exhibits a periodic modulation of density along the y axis in the crossing plane at a wavelength scale. To determine the spatial period of the plasma grating, we consider the interaction of two laser beams crossing at an angle 2θ, as shown in Fig. 1. The propagation vectors of the two beams can be represented as $\mathbf{k}_1 = \hat{\boldsymbol{z}}\, k \cos\theta - \hat{\boldsymbol{y}}\, k \sin\theta$ and $\mathbf{k}_2 = \hat{\boldsymbol{z}}\, k \cos\theta + \hat{\boldsymbol{y}}\, k \sin\theta$, where $k = \omega/c$ is the wavenumber, ω is the angular frequency, c is the speed of light in vacuum, and $\hat{\boldsymbol{x}}$, $\hat{\boldsymbol{y}}$, $\hat{\boldsymbol{z}}$ are unit vectors in the x, y, z directions. We assume that the two beams are plane waves and have the same amplitude and frequency. They irradiate the plasma at incidence angles θ and $-\theta$ with respect to the z axis. The electric fields of the two beams can then be written in the forms

$$\mathbf{E}_1(\mathbf{r}_1, t) = \mathbf{E}_0 \exp[i(\mathbf{k}_1 \cdot \mathbf{r}_1 - \omega t)], \tag{1}$$

$$\mathbf{E}_2(\mathbf{r}_2, t) = \mathbf{E}_0 \exp[i(\mathbf{k}_2 \cdot \mathbf{r}_2 - \omega t)], \tag{2}$$

Here $\mathbf{E}_0$ represents the common complex amplitude vector of the two beams, $\mathbf{r}_1$ and $\mathbf{r}_2$ are the spatial position vectors, and ω is the angular frequency. In the region of overlap, we have $\mathbf{r}_1 = \mathbf{r}_2 = \mathbf{r}$, and the electric field can be expressed as

$$\mathbf{E}(\mathbf{r}, t) = \mathbf{E}_1(\mathbf{r}, t) + \mathbf{E}_2(\mathbf{r}, t) = \mathbf{E}_0[\exp(i\mathbf{k}_1 \cdot \mathbf{r} - i\omega t) + \exp(i\mathbf{k}_2 \cdot \mathbf{r} - i\omega t)]. \tag{3}$$

The intensity related to the two overlapping waves is

$$I(\mathbf{r}, t) = |\mathbf{E}(\mathbf{r}, t)|^2 = |\mathbf{E}_0[\exp(i\mathbf{k}_1 \cdot \mathbf{r} - i\omega t) + \exp(i\mathbf{k}_2 \cdot \mathbf{r} - i\omega t)]|^2$$

$$= |\mathbf{E}_0|^2[2 + \exp(i\mathbf{k}_1 \cdot \mathbf{r} - i\mathbf{k}_2 \cdot \mathbf{r}) + \exp(i\mathbf{k}_2 \cdot \mathbf{r} - i\mathbf{k}_1 \cdot \mathbf{r})]. \tag{4}$$

Substituting $\mathbf{k}_1$ and $\mathbf{k}_2$ into Eq. (4) gives

$$I(\mathbf{r}, t) = |\mathbf{E}_0|^2[2 + \exp(-2iky \sin\theta) + \exp(2iky \sin\theta)]. \tag{5}$$

This simplified expression describes the intensity distribution of the standing wave field formed by the crossing propagation of two lasers with the same frequency and amplitude. The intensity

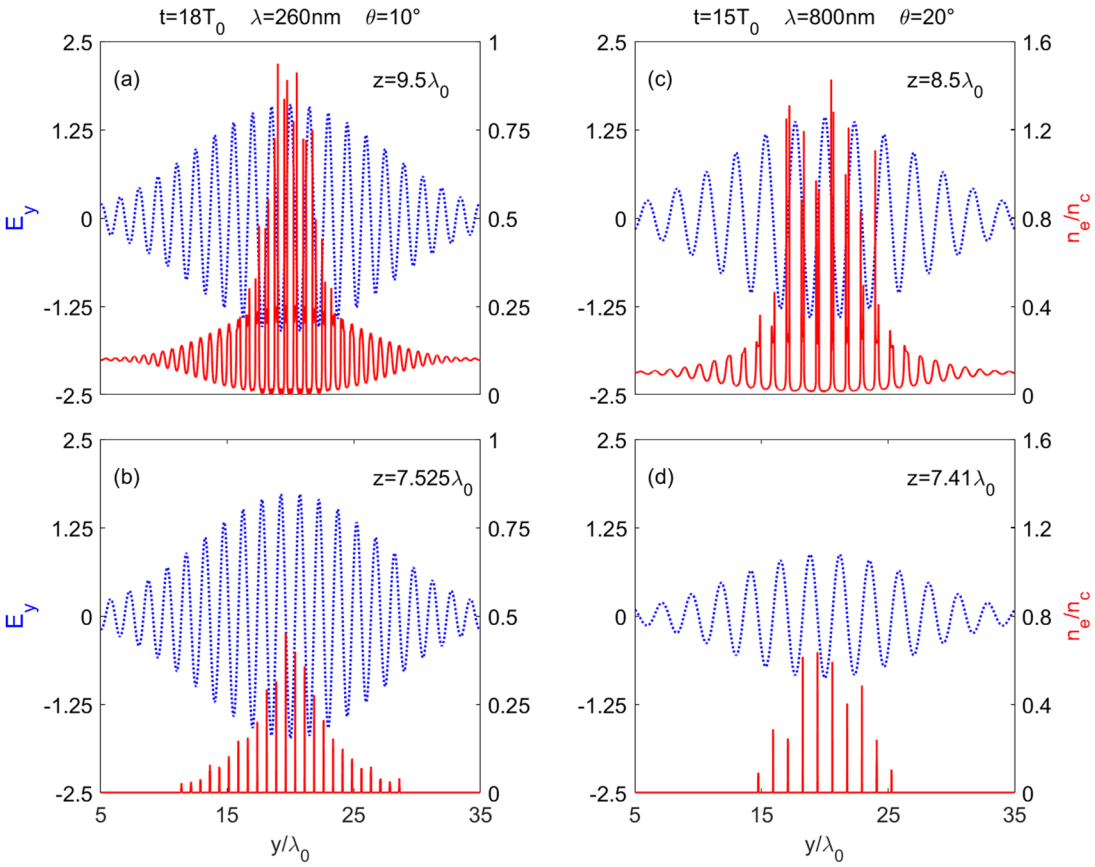

FIG. 4. Normalized laser light field (blue dotted lines) and electron density (red solid lines) along the y axis at different positions for two different scenarios. In (a) and (b), ultraviolet femtosecond laser light (λ = 260 nm) is used at a fixed angle of incidence of $\theta = 10°$. (c) and (d) show the femtosecond laser light (λ = 800 nm) at time $t = 15T_0$ when the angle of incidence is modified to $\theta = 20°$.

I exhibits a periodic modulation along the y axis with wave vector $q = 2k \sin\theta = 2\pi/\Lambda$. Consequently, the ponderomotive force will induce a periodic modulation of the electron density with a spatial period $\Lambda = \lambda/(2\sin\theta)$. It is evident that the period of the plasma grating is determined solely by the wavelength of the laser and the angle of incidence. Specifically, for $\theta = 10°$ and $\lambda = 800$ nm, we can deduce that the period of the plasma grating is ~2.3 μm, which is highly consistent with the simulation results obtained in Sec. II.

To demonstrate the influence of laser wavelength and incident angle on the formation of the EBC, we conducted additional simulations for comparison, as shown in Fig. 4. In Fig. 4(a), we used a laser wavelength of $\lambda = 260$ nm while keeping the other laser and plasma parameters the same as in the previous simulations. It is observed that the periods of both the electron grating and the electron beams are shorter than those in Fig. 3. The density of the individual electron beams decreases to ~$0.5n_c$, and their width is compressed to about 10 nm. However, owing to the limitations of current laser technology, it is challenging to implement this experiment.

In Fig. 4(c), we changed the angle of incidence to $\theta = 20°$ while keeping the other parameters constant. We observe that the periods of both the electron grating and the electron beams are again shorter than those in Fig. 3. This result further confirms that the laser wavelength and angle of incidence are crucial factors that influence the periods of the plasma grating and electron beams. From the formula in Eq. (5) for the intensity of the standing wave, it is evident that this intensity exhibits a periodic relationship with respect to the incident angle, rather than a linear one. Consequently, the density and width of the generated electron beams also display oscillatory behavior with respect to the angle of incidence. For instance, when we varied the angle of incidence from $\theta = 5°$ to $\theta = 50°$ while keeping other parameters constant, the simulation results were in agreement with the predictions from Eq. (5). Considering that the period of the plasma grating is $\Lambda = \lambda/(2\sin\theta)$, it is evident that the angle of incidence should not be too small. If the angle is approximately zero, then the two laser beams will no longer interfere, leading to the absence of electron beam generation.

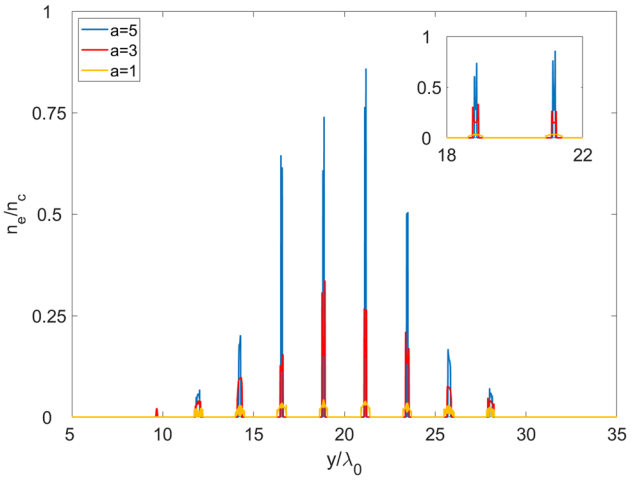

FIG. 5. Normalized electron density along the y axis for laser strengths $a_L = 1$ (yellow solid line), $a_L = 3$ (red solid line), and $a_L = 5$ (blue solid line).

To investigate the influence of laser intensity on the EBC, Fig. 5 compares the peak density of the electron beams for three different laser field strengths. The results indicate that the period of the electron beams is not affected by the laser intensity. This supports the previous finding that only the laser wavelength and incident angle play a role in determining the period of the electron beams. It is observed that the peak density of the electron beams increases with increasing laser field strength, reaching $0.86n_c$ for $a_L = 5$ and $0.04n_c$ for $a_L = 1$. This trend can be attributed to the stronger ponderomotive force arising with higher-intensity lasers, which determines the density of the electron grating. Consequently, continuous Coulomb expansion is more likely to occur. Therefore, the generation of an EBC requires a sufficiently intense laser to expel electrons and create electron cavities that facilitate Coulomb expansion. The simulations also reveal that higher laser intensities result in a narrower compression of the electron beam, indicating a smaller scale in the y direction. Additional simulations were conducted to explore the impact of different laser durations on the generation of the EBC. The results are similar to those shown in Fig. 3.

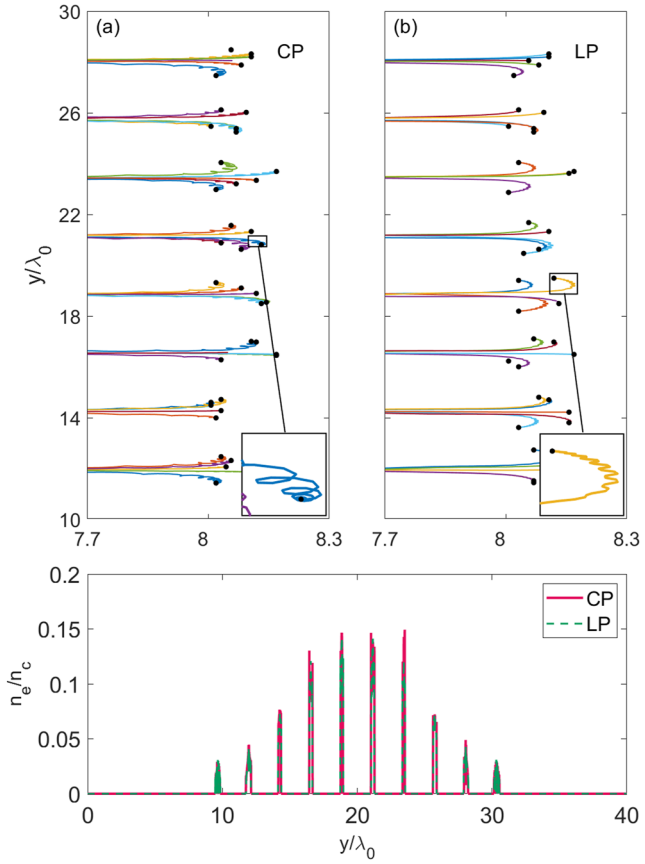

FIG. 6. Trajectories of electrons in the EBC for (a) circularly and (b) linearly polarized laser pulses with the same laser intensity. The black dots represent the starting points of the electron trajectories. In (c), the normalized electron density of EBC along the y axis is presented, using the same laser and plasma parameters as in (a) and (b).

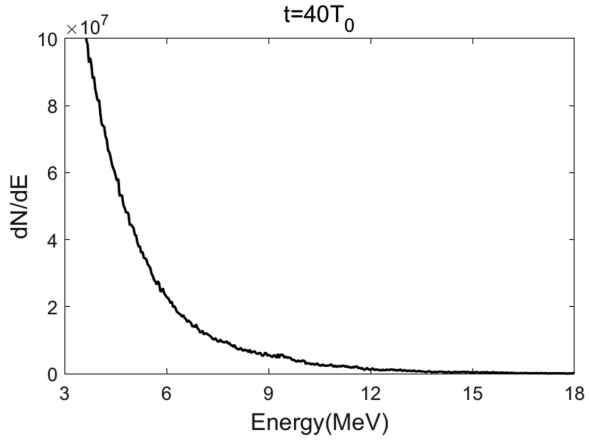

FIG. 7. Energy spectrum of EBC at $t = 40T_0$.

IV. TRANSPORTATION OF EBC

To further investigate the mechanism of generation of the EBC, we tracked the trajectories of several groups of electrons that were induced by circularly polarized (CP) and linearly polarized (LP) laser pulses with the same laser intensity, as shown in Fig. 6. Our results demonstrate that both CP and LP laser pulses are capable of generating the EBC phenomenon. As already mentioned, during the formation of the plasma grating, the ponderomotive force initially pushes the electrons to form high-density peaks. The local charge non-neutrality between electrons and ions causes the electrons to experience a Coulomb expansion. Subsequently, some of the electrons expand into the vacuum region. We can observe from the electron trajectories in Fig. 6 that during the initial stage, under the influence of the laser polarization, the electrons move forward in a spiral pattern for CP laser pulses and in a zigzag pattern for LP laser pulses. Once the electrons expand into the vacuum, they become trapped by the stationary wave that forms along the y direction when the two laser pulses intersect on the plasma target. As a result, the EBC can be collimated and guided by the stationary wave for tens of femtoseconds. Furthermore, we compared the peak density of the electron bunches between CP and LP lasers and obtained similar results, as shown in Fig. 6(c). This suggests that laser polarization does not significantly affect the peak density of the electron bunches.

As already mentioned, the Coulomb expansion of the electrons causes the acceleration process. Owing to the continuous action of the ponderomotive force, most electrons accumulate in the electron peaks, resulting in continuation of the acceleration process caused by Coulomb expansion. The energy spectrum of the EBC, as shown in Fig. 7, demonstrates that the electrons are accelerated to energies ranging from ~5 to 20 MeV at time $t \sim 40T_0$.

V. CONCLUSION

In summary, the interaction of two circularly or linearly polarized laser pulses with a uniform under-critical-density plasma can generate a standing wave, leading to the formation of a spatially periodic plasma grating. This grating causes a local charge imbalance, resulting in a significant mutual repulsion among electrons and inducing Coulomb expansion. The guided and focused expansion of electrons into the vacuum leads to the creation of a high-density nanoscale narrow electron beam comb (EBC). The period of the plasma grating and EBC depends on the laser wavelength and incident angle, while the peak density is influenced by various laser parameters. It has been observed that the generation of high-density EBCs requires a broad range of specific laser and plasma parameters, suggesting the potential for stable EBC generation. Remarkably, these EBCs can propagate stably in vacuum for several tens of femtoseconds. They can serve as a valuable source of high-brightness short-pulse coherent radiation, including x-rays and gamma rays, enabling the exploration of ultrafast processes at the molecular level. Furthermore, the expansion process of electrons in the standing wave can generate x-ray and terahertz radiation, and the tunable standing wave can be used as the wiggler for a short-wavelength free-electron laser. However, further research is needed to gain a detailed understanding of the expansion process and higher-dimensional effects associated with this mechanism. In conclusion, the mechanism studied here exhibits promising potential for various applications and warrants further investigation.

ACKNOWLEDGMENTS

This work was supported by the National Natural Science Foundation of China (Grant Nos. 12174410, 11991072, 11991074, 12225411, and 12105353), the CAS Project for Young Scientists in Basic Research (Grant No. YSBR060), the State Key Laboratory Program of the Chinese Ministry of Science and Technology, and the CAS Youth Innovation Promotion Association (Grant Nos. Y201952 and 2022242).

AUTHOR DECLARATIONS

Conflict of Interest

The authors have no conflicts to disclose.

Author Contributions

Hetian Yang: Data curation (equal); Formal analysis (equal); Investigation (equal). **Jingwei Wang**: Conceptualization (equal). **Shixia Luan**: Conceptualization (lead); Data curation (lead); Formal analysis (lead); Investigation (lead); Supervision (equal); Writing – original draft (lead). **Ke Feng**: Conceptualization (equal). **Wentao Wang**: Formal analysis (equal); Supervision (equal); Writing – review & editing (equal). **Ruxin Li**: Supervision (equal).

DATA AVAILABILITY

The data that support the findings of this study are available from the corresponding author upon reasonable request.

REFERENCES

[1] J. F. Federici, "Review of four-wave mixing and phase conjugation in plasmas," IEEE Trans. Plasma Sci. **19**, 549 (1991).

[2] J. Faure, C. Rechatin, A. Norlin, A. Lifschitz, Y. Glinec, and V. Malka, "Controlled injection and acceleration of electrons in plasma wakefields by colliding laser pulses," Nature **444**, 737 (2006).

[3]L. Yang, Z. G. Deng, M. Y. Yu, and X. G. Wang, "High-charge energetic ions generated by intersecting laser pulses," Phys. Plasmas **23**, 083106 (2016).
[4]L. Yang, Z. Deng, C. Jiang, F. Yang, and R. Ma, "High-charge energetic electron bunch generated by multiple intersecting lasers," Phys. Plasmas **25**, 083102 (2018).
[5]J. Elle, T. Z. Zhao, Y. Ma, K. Behm, A. Lucero, A. Maksimchuk, J. A. Nees, A. G. R. Thomas, A. Schmitt-Sody, and K. Krushelnick, "Multi-electron beam generation using co-propagating, parallel laser beams," New J. Phys. **20**, 093021 (2018).
[6]R. Lehe, A. F. Lifschitz, X. Davoine, C. Thaury, and V. Malka, "Optical transverse injection in laser-plasma acceleration," Phys. Rev. Lett. **111**, 085005 (2013).
[7]L. Reichwein, A. Pukhov, and M. Buscher, "Acceleration of spin-polarized proton beams via two parallel laser pulses," Phys. Rev. Accel. Beams **25**, 081001 (2022).
[8]Y. X. Zhang, S. Rykovanov, M. Shi, C. L. Zhong, X. T. He, B. Qiao, and M. Zepf, "Giant isolated attosecond pulses from two-color laser-plasma interactions," Phys. Rev. Lett. **124**, 114802 (2020).
[9]L. L. Zhang, W. M. Wang, T. Wu, R. Zhang, S. J. Zhang, C. L. Zhang, Y. Zhang, Z. M. Sheng, and X. C. Zhang, "Observation of terahertz radiation via the two-color laser scheme with uncommon frequency ratios," Phys. Rev. Lett. **119**, 235001 (2017).
[10]Z. Zhang, Y. Chen, M. Chen, Z. Zhang, J. Yu, Z. Sheng, and J. Zhang, "Controllable terahertz radiation from a linear-dipole array formed by a two-color laser filament in air," Phys. Rev. Lett. **117**, 243901 (2016).
[11]Z. M. Sheng, J. Zhang, and D. Umstadter, "Plasma density gratings induced by intersecting laser pulses in underdense plasmas," Appl. Phys. B **77**, 673 (2003).
[12]S.-X. Luan, Q.-J. Zhang, and W.-L. Gui, "Plasma Bragg gratings generated by the interaction of two counter-propagating laser pulses with plasmas," Acta Phys. Sin. **57**, 7030 (2008).
[13]H. H. Ma, S. M. Weng, P. Li, X. F. Li, Y. X. Wang, S. H. Yew, M. Chen, P. McKenna, and Z. M. Sheng, "Growth, saturation, and collapse of laser-driven plasma density gratings," Phys. Plasmas **27**, 073105 (2020).
[14]G. Lehmann and K. H. Spatschek, "Reflection and transmission properties of a finite-length electron plasma grating," Matter Radiat. Extremes **7**, 054402 (2022).
[15]Z. H. Wu, Y. L. Zuo, X. M. Zeng, Z. L. Li, Z. M. Zhang, X. D. Wang, B. L. Hu, X. Wang, J. Mu, J. Q. Su, Q. H. Zhu, and Y. P. Dai, "Laser compression via fast-extending plasma gratings," Matter Radiat. Extremes **7**, 064402 (2022).
[16]H. C. Wu, Z. M. Sheng, Q. J. Zhang, Y. Cang, and J. Zhang, "Manipulating ultra-short intense laser pulses by plasma Bragg gratings," Phys. Plasmas **12**, 113103 (2005).
[17]H. C. Wu, Z. M. Sheng, and J. Zhang, "Chirped pulse compression in nonuniform plasma Bragg gratings," Appl. Phys. Lett. **87**, 201502 (2005).
[18]A. D. Lad, Y. Mishima, P. K. Singh, B. Y. Li, A. Adak, G. Chatterjee, P. Brijesh, M. Dalui, M. Inoue, J. Jha, S. Tata, M. Trivikram, M. Krishnamurthy, M. Chen, Z. M. Sheng, K. A. Tanaka, G. R. Kumar, and H. Habara, "Luminous, relativistic, directional electron bunches from an intense laser driven grating plasma," Sci. Rep. **12**, 16818 (2022).
[19]L. P. Shi, W. X. Li, Y. D. Wang, X. Lu, L. E. Ding, and H. P. Zeng, "Generation of high-density electrons based on plasma grating induced Bragg diffraction in air," Phys. Rev. Lett. **107**, 095004 (2011).
[20]Q. Chen, D. Maslarova, J. Z. Wang, S. X. Lee, V. Horny, and D. Umstadter, "Transient relativistic plasma grating to tailor high-power laser fields, wakefield plasma waves, and electron injection," Phys. Rev. Lett. **128**, 164801 (2022).
[21]H. Xu, W. W. Chang, H. B. Zhuo, L. H. Cao, and Z. W. Yue, "Parallel programming of 2 1/2-dimensional pic under distributed-memory parallel environments," Chin. J. Comput. Phys **19**, 305 (2002).